

Supporting Information

Achieving fast and stable Li⁺ transport in lithium-sulfur battery via a high ionic conduction and high adhesion solid polymer electrolyte

Ximing Cui, Xiaohui Wang, Qinmin Pan

School of Chemistry and Chemical Engineering, Harbin Institute of Technology,
Harbin 150001, China.

Correspondence to: Prof. Qinmin Pan, School of Chemistry and Chemical Engineering, Harbin Institute of Technology, Harbin 150001, China. E-mail: panqm@hit.edu.cn

1. Experimental

1.1 Preparation of the PO-PU-LiTFSI electrolyte:

To prepare the PO-PU-LiTFSI electrolyte, 1g of polyethylene glycol (PEG; Aladdin, Mw=100~10000) and 80 μ l of M-diisocyanate were dissolved in 10 ml of acetonitrile (ACN; Aladdin, \geq 99.9%, Mw=222.32). After stirring at 60°C for 5 h, bis(trifluoromethane)sulfonimide lithium salt (LiTFSI; Aladdin, 99%) was added to the above solution. The resulting solution (PU-LiTFSI solution) was coated onto polyolefin (PO) membrane and then placed in an oven at 60°C for 12 h to obtain the PO-PU-LiTFSI electrolyte. PO membrane was purchased from Asahi Chemical Industry Co. Ltd. The thickness of the PO membrane is about 16 μ m. The porosity of the PO membrane is about 45%. The molecular weight and Polydispersity index were analyzed by gel permeation chromatography (GPC). After 5 hours of reaction, the resulting molecular weight of the synthesized PU was 406083 and polydispersity index was 2.0360 (Figure S12). For comparison,

polyethylene oxide (PEO; Aladdin, average $M_v=600000$) and LiTFSI were dissolved in acetonitrile. The resulting solution (PEO-LiTFSI solution) was coated onto PO membrane and then the membrane was placed in an oven at 60°C for 12 h to obtain PO-PEO-LiTFSI electrolyte. In order to avoid side-reactions of MDI during PU synthesis, the acetonitrile was treated using molecular sieves for 1 day to remove water from it and the above operations were all carried out in an argon atmosphere.

1.2 Preparation of sulfur cathodes and assembly of solid-state batteries:

Carbon black and sulfur powder were heat at 155°C for 12 h to form a sulfur-carbon composite. Then the composite, conductive carbon material, PU-LiTFSI solution and binder were mixed in the solution of n-propanol (Aladdin, $\geq 99.9\%$) and water to form a uniform slurry. The slurry was coated on current collectors (Al foil or nickel foam), and dried in a vacuum oven at 40°C for 12 h to obtain sulfur cathodes (Sulfur loading: 1~5 mg cm⁻²). Then the PU-LiTFSI solution was coated on the obtain sulfur cathodes, and the cathodes were placed in an oven at 60°C for 12 h. The as-prepared sulfur cathodes, PO-PU-LiTFSI electrolytes and lithium foils were assembled into coin cells or pouch cells. The above operations were all carried out in a glovebox ($O_2 < 0.1$ ppm, $H_2O < 0.1$ ppm).

Characterizations: Scanning electron microscope (SEM) images were observed using a Zeiss Supra 55. Fourier Transform infrared (FT-IR) spectra were tested by a Nicolet is50 spectroscope. X-ray diffraction (XRD) patterns were recorded using a X'PERT PRO diffractometer. Thermogravimetric analysis (TGA) curves were recorded using a TG209F3 thermal gravimetric analyzer. Differential scanning calorimetry (DSC) curves were tested using a DSC200F3 differential scanning calorimeter. Puncture strength and tensile strength curves of the electrolytes were tested by a CREE 8007B

universal electromechanical testing machine. During the puncture strength test, a steel needle with a diameter of 0.4 mm was used for puncture, and the puncture speed was (50 ± 5) mm min⁻¹.

1.3 Adhesive force measurement:

Adhesive force between the electrolyte and electrode was measured by a sensor (Me-systeme, K3D40 2N). First, the electrolyte was fixed on the sensor. A force of 12 N was applied to allow the electrode and electrolyte to tight contact, and then the electrolyte was detached from the electrode. The maximal force during the detachment was defined as the adhesive force. The contact area between the electrode and the electrolyte was 1.5 cm² and the detachment speed of the electrolyte was 1 mm s⁻¹.

1.4 In-situ laser confocal microscope observation:

The sulfur cathode, PO-PU-LiTFSI electrolyte and lithium foil were sandwiched in a quartz cell. The anodes and cathodes were connected with nickel wires. The cell was sealed by epoxy resin. The electrode/electrolyte interfaces were in-situ observed by a 3D measuring laser microscope (OLS4100 OLYMPUS).

1.5 Electrochemical measurements:

All solid-state batteries were measured at ~30°C. Ionic conductivity, electrochemical window and lithium ion transference number were all measured on a CHI 660e.

The ionic conductivity (σ) of the electrolyte was calculated by the following formula

$$\sigma = \frac{L}{R_b \cdot S}$$

where L (cm) is the thickness of the electrolyte, R_b is the bulk resistance (Ω) of the electrolyte and S is the contact area between the electrolyte and electrode.

The activation energy (E_a) was fitted using the Arrhenius equation by the following formula

$$\sigma = \sigma_0 \exp\left(-\frac{E_a}{RT}\right)$$

where σ_0 is a pre-exponential factor and R is the ideal gas constant.

The electrochemical window was measured by linear sweep voltammetry in the open-circuit voltage range up to 5 V. An asymmetrical cell using the PO-PU-LiTFSI electrolyte was used for testing. Scan rate was 0.1 mV S⁻¹.

The lithium ion transference number was calculated by the following formula

$$t_{Li^+} = \frac{I_s(\Delta V - I_0 R_0)}{I_0(\Delta V - I_s R_s)}$$

a symmetrical Li||Li cell using the PO-PU-LiTFSI electrolyte was used for testing. Where I_0 and R_0 are the current density and interfacial resistance of the symmetric cell before polarization. DC polarization voltage (ΔV) is 10 mV. I_s and R_s are the current density and interfacial resistance of the symmetric cell after polarization.

The lithium ion diffusion coefficient (D_{Li^+}) was estimated using the method proposed by Ma *et al.* by the following formula

$$D_{Li^+} = \frac{Slope \times L^2}{\pi^2}$$

a symmetrical Li||Li cell using the PO-PU-LiTFSI electrolyte was used for testing.¹ Where L is the thickness of the PO-PU-LiTFSI electrolyte.

All coin cells and pouch cells were tested on Neware battery testing systems.

1.6 Computational Details:

The adsorption binding energy (E_{ads}) was calculated using density functional theory (DFT) with the Perdew-Burke-Ernzerhof (PBE) functional of generalized gradient approximation (GGA) with the DNP basis set (basfile_v4.4) in the DMol3 package as follows

$$E_{ads} = E_x + E_y - E_{x+y}$$

where E_{x+y} represents total energy of the adsorbed system. E_x and E_y represent total energy of the substrate and adsorbate, respectively.

The energy barrier calculations were carried out by using the Vienna ab initio Simulation Package (VASP) code. The projected augmented wave (PAW) potentials were applied to describe the ionic cores. The exchange and correlation energies were evaluated using the PBE functional. The Climbing Image-Nudged Elastic Band (CI-NEB) methods were employed to calculate the migration barriers in structures. The kinetic energy cutoff was set at 500 eV. All the atoms were relaxed until the residual forces were less than 0.01 eV \AA^{-1} and the total energy difference was less than 10^{-5} eV .

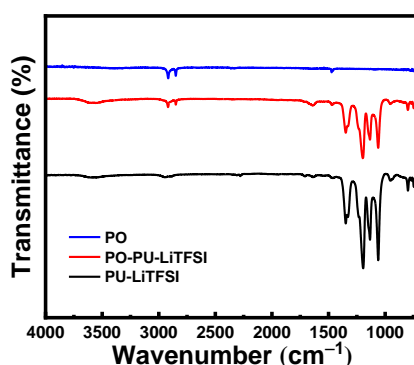


Figure S1. FTIR spectra of the PO, PO-PU-LiTFSI and PU-LiTFSI.

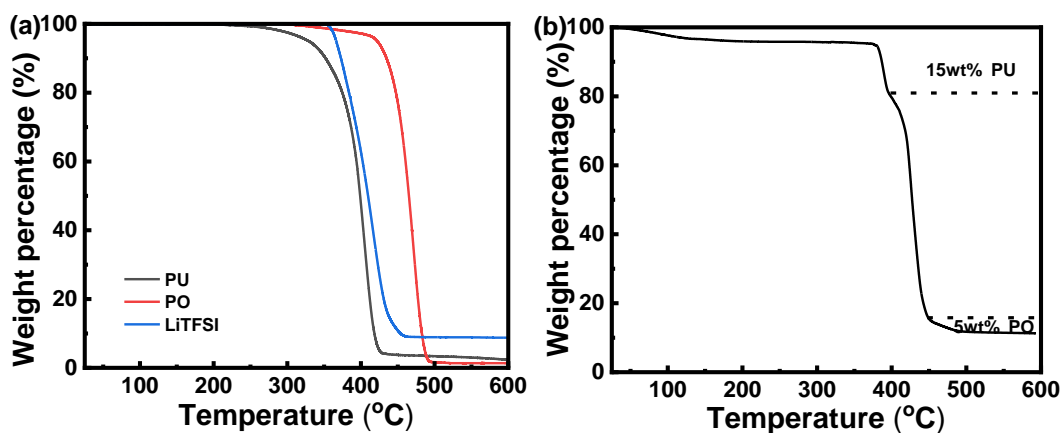


Figure S2. a, b) TGA curves of the PO, PU, LiTFSI and PO-PU-LiTFSI electrolyte.

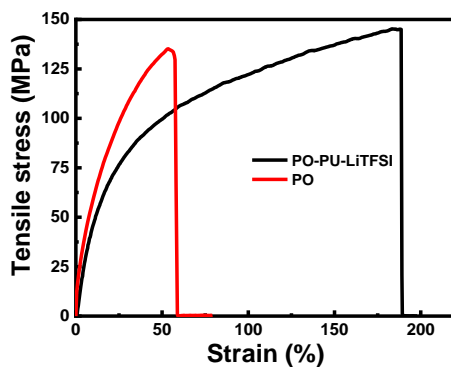


Figure S3. Tensile stress-strain curves of the PO-PU-LiTFSI electrolyte and PO membrane.

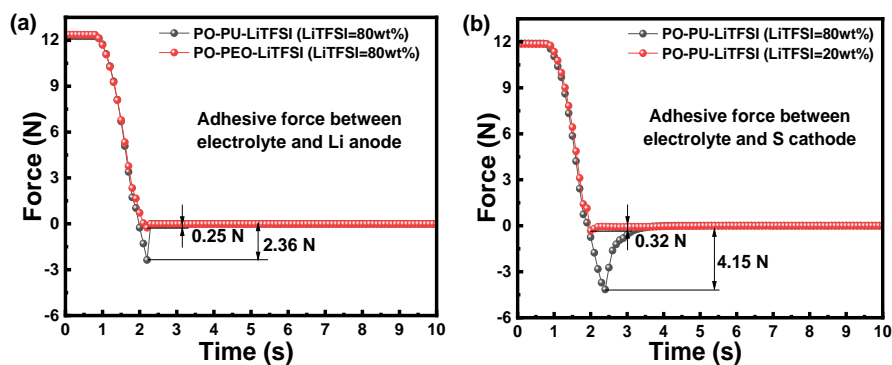


Figure S4. a) Measurements of the adhesive force between different electrolytes and Li anodes. b)

Measurements of the adhesive force between different electrolytes and sulfur cathodes.

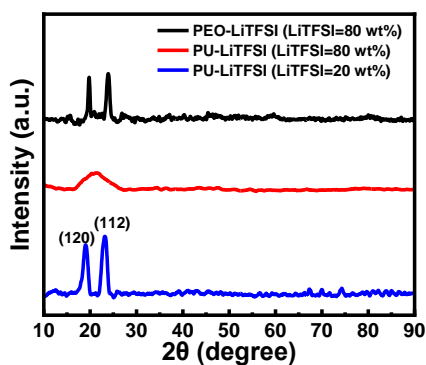


Figure S5. XRD patterns of PEO-LiTFSI and PU-LiTFSI with different LiTFSI content.

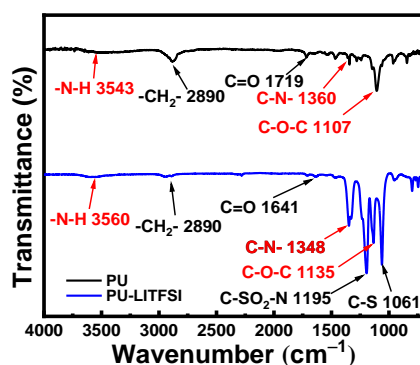


Figure S6. FTIR spectra of PU and PU-LiTFSI.

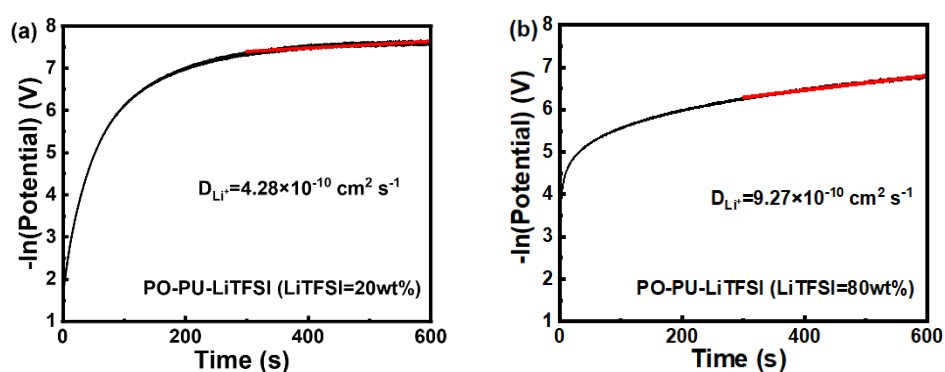


Figure S7. Diffusion coefficient measurement of the PO-PU-LiTFSI electrolytes using the restricted diffusion method. a, b) Logarithm of potential vs. time of the cells using the PO-PU-LiTFSI electrolytes with different LiTFSI content.

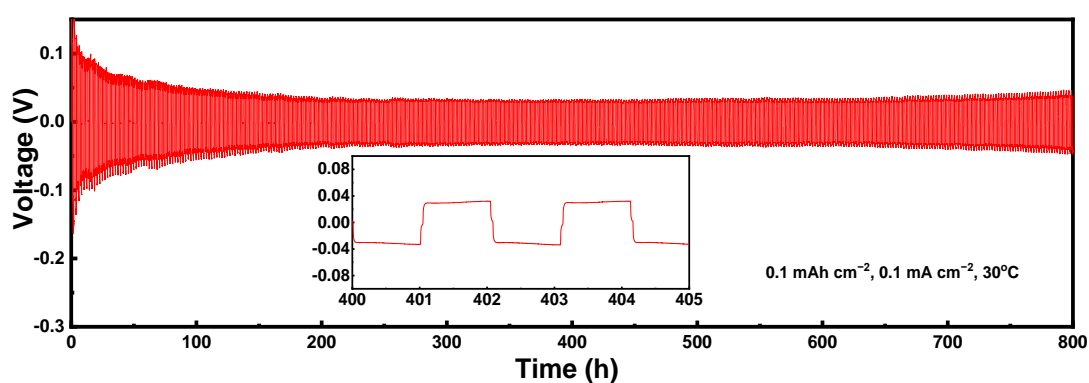


Figure S8. Voltage profile of the symmetric Li||Li cell using the PO-PU-LiTFSI electrolyte. The LiTFSI content of the electrolyte is 80wt%.

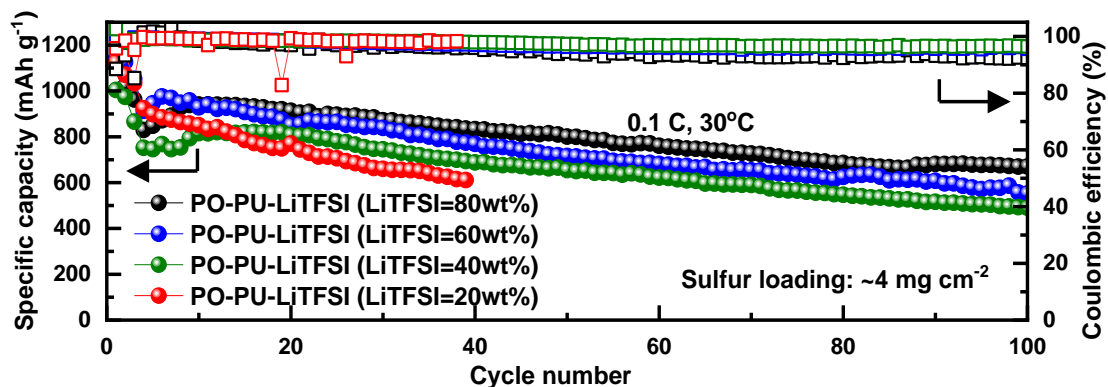


Figure S9. Cycling performances of Li-S batteries using the PO-PU-LiTFSI electrolytes with different LiTFSI content.

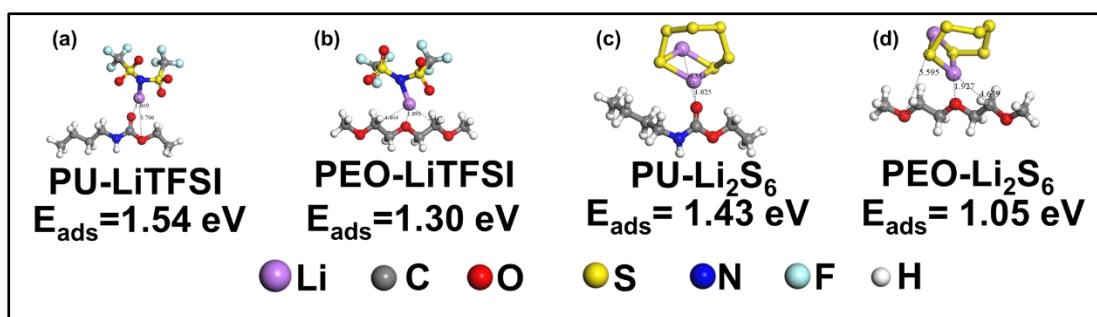


Figure S10. DFT calculation results of the adsorption binding energy between a) LiTFSI and PU, b) LiTFSI and PEO, (c) Li₂S₆ and PU, (d) Li₂S₆ and PEO.

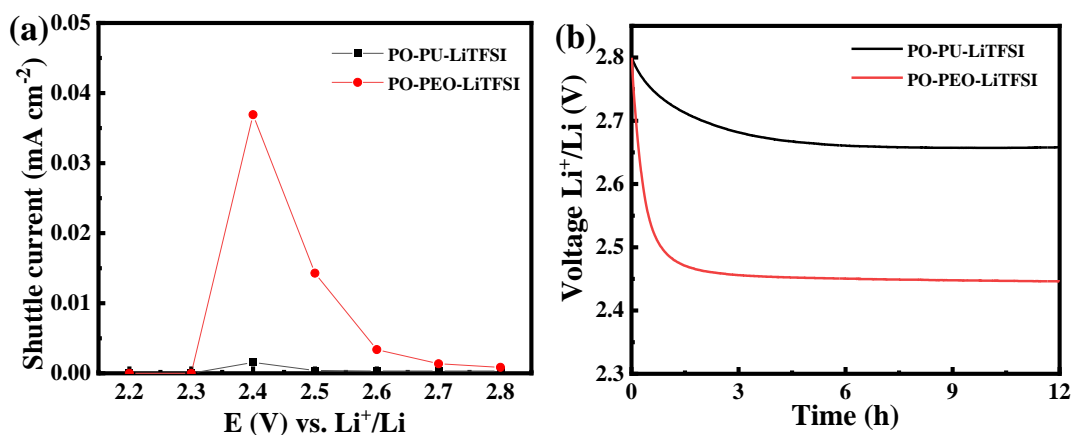


Figure S11. (a) Shuttle current and (b) self-discharge rate at OCV of the Li-S batteries using different electrolytes.

Table S1. Comparison on the electrochemical performances of the Li-S batteries using different solid-state electrolytes.

Electrolytes	Ionic conductivity/ S cm ⁻¹	Tensile stress/ MPa	Li-ion transfer number	Cycling performance/ mAh g ⁻¹	Ref.
PEO/LiTFSI/iCP@TFSI	9.5×10 ⁻⁶ (30°C)	1	0.43	610(125th cycle) (0.1 C, 30°C, 0.8 mg cm ⁻¹)	2
PEO/LiTFSI/LLTO	2.3×10 ⁻⁴ (25°C)	2	--	384(50th cycle) (0.05 C, 30°C, 1.3 mg cm ⁻¹)	3
PEO/LiTFSI/IL@ZrO ₂	4.1×10 ⁻⁴ (37°C)	--	0.45	600(80th cycle) (0.1 C, 37°C, 1.2 mg cm ⁻¹)	4
PEO/Li ₄ (BH ₄) ₃ I/SiO ₂	4.3×10 ⁻⁴ (70°C)	--	0.62	967(75th cycle) (0.1 C, 70°C)	5
PEO/LiTFSI/LATP	4.0×10 ⁻⁵ (30°C)	--	0.27	784(120th cycle) (0.1 C, 75°C, 1 mg cm ⁻¹)	6
PEO/LiTFSI/PTFE	--	--	--	630(60th cycle) (0.05 mA cm ⁻¹ , 55°C, 1 mg cm ⁻¹)	7
PVDF/LLBZTO/LiF	3.4×10 ⁻⁴ (20°C)	--	--	610(80th cycle) (0.1 C, 20°C, 0.5 mg cm ⁻¹)	8
PEO/LiDFTFSI	2.0×10 ⁻⁴ (70°C)	--	--	600 (30th cycle) (0.1 C, 70°C, 1 mg cm ⁻¹)	9
This work	1.8×10⁻⁴(30°C)	145	0.54	610(125th cycle) (0.1C, 30°C, 4 mg cm⁻¹)	--

Table S2. EIS fitting result of the solid-state Li-S batteries using the PO-PU-LiTFSI electrolytes with different LiTFSI content after different cycles.

		5th	10th (Ω)	20th (Ω)	30th (Ω)	40th (Ω)	80th (Ω)
PO-PU-LiTFSI (LiTFSI=80wt%)	<i>R_o</i>	6	4.7	5.7	4.4	5.2	5.6
	<i>R_{SEI}</i>	7.7	4.4	4.6	3.4	3.8	3.3
	<i>R_{ct}</i>	17.64	10	7.4	5.9	5.9	4.3
PO-PU-LiTFSI (LiTFSI=20wt%)	<i>R_o</i>	4.7	6	5.6	12.1	7.6	-
	<i>R</i>	5.4	7.9	7.1	14.2	7.4	-
	<i>R_{SEI}</i>	10.3	24.1	13.1	46.3	17.9	-
	<i>R_{ct}</i>	14.24	28.31	16.1	45.9	19.1	-

Supplementary references

1. Ma YP, Doyle M, Fuller TF, et al. The Measurement of a Complete Set of Transport Properties for a Concentrated Solid Polymer Electrolyte Solution. *J. Electrochem. Soc.* 1995; 142: 1859-68. DOI:.
2. Y Wang, HF Ji, XJ Zhang, et al. Cyclopropenium Cationic-Based Covalent Organic Polymer-Enhanced Poly(ethylene oxide) Composite Polymer Electrolyte for All-Solid-State Li-S Battery. *ACS Appl. Mater. Interfaces* 2021; 13: 16469-77. DOI: 10.1021/acscami.1c02309.
3. P Zhu, CY Yan, JD Zhu, et al. Flexible Electrolyte-Cathode Bilayer Framework with Stabilized Interface for Room-Temperature All-Solid-State Lithium-Sulfur Batteries. *Energy Stor. Mater.* 2019; 17: 220-5. DOI: 10.1016/j.ensm.2018.11.009.
4. OW Sheng, CB Jin, JM Luo, et al. Ionic Conductivity Promotion of Polymer Electrolyte with Ionic Liquid Grafted Oxides for All-Solid-State Lithium-Sulfur Batteries. *J. Mater. Chem. A* 2017; 5: 12934-42. DOI: 10.1039/c7ta03699j.
5. Zhang X, Zhang TF, Shao YF, et al. Composite Electrolytes Based on Poly(Ethylene Oxide) and Lithium Borohydrides for All-Solid-State Lithium-Sulfur Batteries. *ACS Sustainable Chem. Eng.* 2021; 9: 5396-404. DOI: 10.1021/acssuschemeng.1c00381.
6. Wang Y, Wang GX, He PG, et al. Sandwich Structured NASICON-Type Electrolyte Matched with Sulfurized Polyacrylonitrile Cathode for High Performance Solid-State Lithium-Sulfur Batteries. *Chem. Eng. J.* 2020; 393: 124705. DOI: 10.1016/j.cej.2020.124705.
7. Fang RY, Xu HH, Xu BY, et al. Goodenough, Reaction Mechanism Optimization of Solid-State Li-S Batteries with a PEO-Based Electrolyte. *Adv. Funct. Mater.* 2021; 31: 2001812. DOI: 10.1002/adfm.202001812.

8. Bag S, Zhou CT, Kim PJ, et al. LiF Modified Stable Flexible PVDF-Garnet Hybrid Electrolyte for High Performance All-Solid-State Li-S Batteries. *Energy Stor. Mater.* 2020; 24: 198-207.
DOI: 10.1016/j.ensm.2019.08.019.
9. Zhang H, Oteo U, Judez X, et al. Designer Anion Enabling Solid-State Lithium-Sulfur Batteries. *Joule* 2019; 3: 1689-702. DOI: 10.1016/j.joule.2019.05.003.